Composite Structures 149 (2016) 33–40

Contents lists available at ScienceDirect

Composite Structures

journal homepage: www.elsevier.com/locate/compstruct

An experimental investigation into multi-scale damage progression in laminated composites in bending

D.J. Mortell [a], D.A. Tanner [b], C.T. McCarthy [a,*]

[a] IComp, Department of Mechanical, Aeronautical and Biomedical Engineering, Materials Surface Science Institute, University of Limerick, Limerick, Ireland
[b] Department of Design and Manufacturing Technology, Materials Surface Science Institute, University of Limerick, Limerick, Ireland

ARTICLE INFO

Article history:
Received 17 January 2016
Accepted 28 March 2016
Available online 30 March 2016

Keywords:
Scanning Electron Microscopy (SEM)
Transverse cracking
Damage mechanics
Delamination

ABSTRACT

In laminated composite materials fibre–matrix debonding, as an initial damage mechanism, can initiate a damage sequence that can result in catastrophic failure of its structure by promoting intermediate damage mechanisms. This paper presents an in-depth experimental investigation into each of these damage mechanisms and how they transition from one state to the next, beginning at the micro-scale with fibre–matrix debonding and crack coalescence, to transverse ply fracture at the meso-scale through to formation of macroscopic delamination.

In-situ SEM micro-mechanical testing is used to determine the onset of the aforementioned damage mechanisms and to follow their progression in laminates of both $[0/90]_s$ and $[90/0]_s$ stacking sequences. The damage progression of $[0/90]_s$ specimens is presented first, followed by the more progressive failure of $[90/0]_s$ specimens, yielding an in-depth analysis of both rapid and more progressive damage growth, respectively. The intralaminar cracking and delamination of $[0/90]_s$ laminates was found to be instantaneous and provided limited opportunity to characterise damage progression. For $[90/0]_s$ laminates, damage progression was much more progressive and various factors such as fibre positioning were shown to influence debonding initiation and crack path development before catastrophic failure and so these laminates form the bulk of the analysis presented for this paper.

1. Introduction

When designing structures for the aerospace industry, light-weight and high stiffness material properties are a priority. Laminated carbon fibre reinforced plastic (CFRP) composite materials have been used for a number of decades to meet these demands. The failure mechanisms associated with composite materials are complex, and laminate fracture is known to involve a sequential accumulation of damage under static or fatigue loading [1]. Damage generally initiates at the micro-scale with fibre–matrix debonding which leads to transverse crack growth and delamination, and eventual structural collapse.

Micro-cracking in composite materials can go undetected as the immediate loss in material stiffness is miniscule. However, in certain applications the presence of micro-cracks may constitute a technological failure. For example, micro-cracking of a composite vessel containing a corrosive agent such as sulphuric acid, used in industry to accelerate chemical processes, could allow the entry of the corrosive agent with detrimental effects on the structure [2]. In another example, during testing of the liquid hydrogen composite fuel tanks for the NASA X-33 launch vehicle, it was found that micro-cracks acted as fuel leakage sites. With no solution to this behaviour and considering the obvious risks associated with fuel leakage, the launch vehicle project was cancelled [3], resulting in a major negative impact on technological advancement with astronomical financial losses. Not only are debonding and micro-cracks considered catastrophic failure in certain applications, they also act as nucleation points for other damage mechanisms such as delamination [1,4], which can result in significant loss in load-bearing capacity of a structure. Hence, a deep understanding of composite damage mechanisms, inclusive of all observable damage mechanisms from the micro-scale to the macro scale, is urgently required by industry.

Previous research relating to composite damage mechanisms has generally focussed on a particular damage mechanism in isolation [5–7]. Previous work by the authors using similar testing techniques investigated transverse crack density and delamination lengths in detail [8]. This paper aims to examine the initiation of observable damage and its progression from one damage mechanism to the next in cross-ply laminates under bending loads. Stacking

* Corresponding author at: L1033, Lonsdale Building, University of Limerick, Castletroy, Limerick, Ireland.
E-mail address: Conor.McCarthy@ul.ie (C.T. McCarthy).

http://dx.doi.org/10.1016/j.compstruct.2016.03.054
0263-8223/

sequences are varied to induce intralaminar failure under normal stress, and then shear stress dominated loading. In-situ micro-mechanical testing of composite laminates is used to apply quasi-static mechanical loading, while observing in real-time the progression of damage mechanisms at the micro-scale. In-situ micro-mechanical testing has been shown to be of significant value for determining damage mechanisms in previous research [9,10].

1.1. Problem description

A micro-test tensile stage (Deben™) was used to apply a bending load to composite specimens to induce intralaminar failure. The key components of the micro-tester are shown in Fig. 1 which can apply up to 2 kN of force with a 33 μm/min displacement rate. The span length and distances between the 8 mm diameter loading and support pins for four-point bending are also shown in Fig. 1.

Real-time video footage from the SEM was recorded during testing to identify various failure events at the micro-scale. Failure mechanisms in composite laminates vary depending on ply orientation and stress state. Testing of $[90/0]_s$ and $[0/90]_s$ laminates can be used to characterise intralaminar damage in composites under normal- and shear-stress dominated failure conditions. It should be noted that all reference to normal and shear stresses in this paper are to be considered applied stresses.

2. Materials and methods

2.1. Composite material

The composite material used for all specimens consisted of an isotropic epoxy matrix (Hexcel™ 6376), reinforced with anisotropic carbon fibres (Toho Tenax™ HTA). The laminates were produced using a vacuum assisted autoclave process in which the laminates were cured for two hours at 175 °C and 700 kN/m^2 pressure. Symmetrical cross-ply laminates were prepared with the following stacking sequence: $[90_4/0_7/90_4]$ specimens representing the worst case scenario for the direction of bending as the outer ply block, which sees a high tensile stress, consists of 90° plies with notably poor transverse stiffness; and $[0_4/90_7/0_4]$ specimens representing the best case scenario for the direction of bending, as the 0° plies are much stiffer and can take a much higher tensile load before failure. Both cross-ply layup types were selected to focus primarily on laminates with relatively low 90°/0° ply ratios. Initial crack growth in laminates is easier to observe when there are fewer 90° plies than 0° plies, as the presence of the relatively stiff 0° plies tended to inhibit rapid crack growth in the 90° ply block at low load levels [9]. The number of plies was limited to ensure that the load required to achieve catastrophic failure of the specimens was not greater than the 2 kN limit of the load-cell.

2.2. Sample preparation

Flat, rectangular shaped specimens were machined from the aforementioned larger flat panel using a diamond tipped composite cutting wheel. The thickness of the specimens was approximately 2 mm, and both $[90_4/0_7/90_4]$ and $[0_4/90_7/0_4]$ specimens were cut from the same laminate and polished. Polishing may introduce artefacts observed during in-situ testing which are not representative of the bulk material response. This is particularly true for 0° (longitudinal) fibres on the surface of the laminate which have their cross section and stiffness reduced during the polishing process [11]. To counteract the effects of polymer charging in the SEM in standard high voltage and high vacuum mode, the specimens were sputter-coated with a conductive gold alloy. A deposition current of 15 mA was applied for 30 s to give a deposition coating thickness of 2.5 nm.

2.3. SEM in-situ bending

The micro-tester was located in the chamber of a SEM (JEOL™ JSM-5600) with the electron source directly over the specimen. The SEM acceleration voltage was 15 kV. The specimens were loaded in four-point bending to induce theoretically pure normal loading conditions between the loading pins, and mixed-mode conditions between the loading and support pins.

3. Results and discussion

The majority of the micro-mechanical testing for this study was performed using $[90/0]_s$ laminates due to the favourably slow damage progression, which accumulated until catastrophic failure. For this research, catastrophic failure is considered as the significant loss of load-bearing capacity of the structure, identified as a load drop of 50% from the peak load. Bending of $[0/90]_s$ laminates was also performed to compare failure characteristics with $[90/0]_s$ laminates. However, the rate of damage progression in $[0/90]_s$ specimens made it very difficult to interpret the transition from one damage mechanism to the next.

The following subsections of the results and discussion will explore the failure mechanisms for cross-ply laminates. The rapid damage progression of $[0/90]_s$ specimens is presented first followed by $[90/0]_s$ specimens, from the initiation of fibre–matrix decohesion at the micro-scale, through to transverse cracking at the meso-scale, through to macro-scopic delamination, and finally concluding at catastrophic failure at the macro-scale.

3.1. Damage process for $[0/90]_s$ laminates in bending

The electron micrographs of Fig. 2 show the type of failure seen during four-point bending of $[0/90]_s$ laminates in the 90° ply block

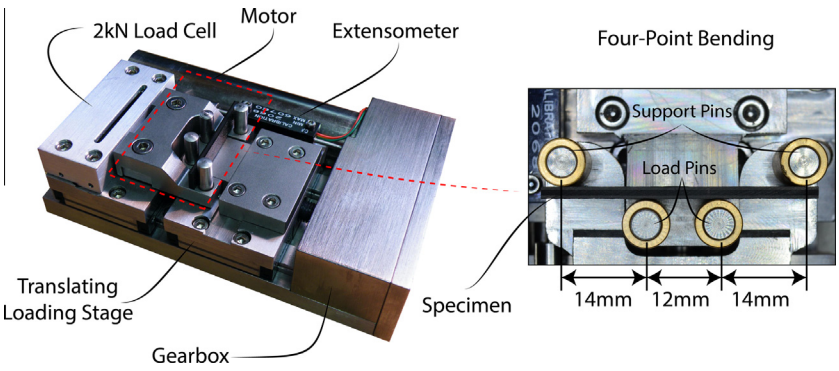

Fig. 1. Overview of Deben 2 kN micro-tester including the drive system and sensors.

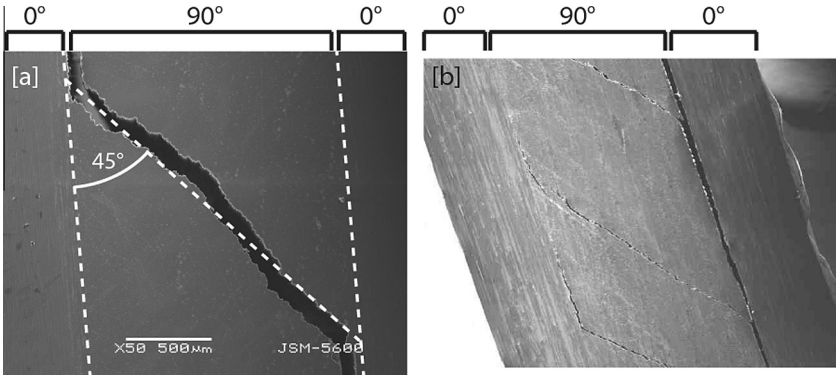

Fig. 2. Electron micrographs of z-shaped cracking from two different samples, with 45° transverse cracking through 90° plies and delamination at both 90°/0° ply boundaries.

between the loading and support pin. The 45° orientation of the failure suggests that the $[0/90]_s$ laminate failure is dominated by the shear stress component, which only exists between the support and loading pins in four-point bending. Prior to the damage seen in these examples, there was no observable indication of damage initiation in the 90° plies or at the 90°/0° ply boundary. This sort of behaviour, in which cracking prior to ultimate failure is completely suppressed, is described in [12] as constrained cracking, which is essentially caused by the high stiffness 0° plies on the exterior of the laminate constraining damage in the transverse ply block, thereby increasing the cracking threshold and hence delaying the onset of damage [13]. Once a certain level of loading had been applied, catastrophic failure of the structure took place instantaneously.

The electron micrographs taken after failure, shown in Fig. 2, show a transverse crack and delaminations at ply boundaries, and followed a z-shaped crack path, which is consistent with shear cracks seen in previous research [14,15]. The angle of the crack through the 90° plies to the 90°/0° ply boundary is approximately 45° (Fig. 2[a]). The 90°/0° ply boundary delamination that resulted from this damage was extensive, and the laminates lost over 50% of their max load carrying capacity, and are then considered failed. In Fig. 2[b], it was observed that a number of 45° cracks through the 90° plies developed approximately 600 µm apart.

A Photron™ Fastcam high frame rate video camera was used to record macro footage of the mechanical failure at 5000 frames per second. From inspection of the resulting video and stills, the entire damage process took place over approximately 0.4 ms. Fig. 3[a] shows the final frame prior to catastrophic failure. Fig. 3[b], taken just after delamination propagation and 0.4 ms after Fig. 3[a], shows the characteristic z-shaped crack path highlighted in Fig. 3 [c]. Of note is the significant gap in the 90° ply block, resulting from this crack growth.

3.2. Damage process for $[90/0]_s$ laminates in bending

A typical load/displacement graph from four-point bending of $[90/0]_s$ laminates is illustrated in Fig. 4. The first phase of the loading history is characterised as the "intralaminar cracking phase" and consists of fibre–matrix debonding, micro-cracking and complete transverse cracking. Completed transverse cracks are marked on the load displacement curve as small temporary drops in load when a transverse crack opens (Fig. 4[a]) [16]. The second phase of the loading history is dominated by delamination as the 90° ply block peels away from the 0° plies. Delamination of the plies eventually leads to catastrophic failure of the structure, as shown in Fig. 4, where a major drop in load is observed.

3.2.1. Fibre–matrix debonding

The initial form of failure observed during mechanical loading was fibre–matrix debonding, as was seen in previous research [17]. This failure is seen in the 90° ply block on the tensile side of the laminate in bending, indicated in the bending diagram of Fig. 5. Interface debonds [a], [b], [c] and [d] are highlighted in Fig. 5 and it was observed that the debond lengths increased with further loading. The debond at Fig. 5[a] is located at the part of the interface closest to an adjacent fibre where the tensile loading direction is perpendicular to the debond and encourages failure at that location. Maligno et al. [18] found that when fibres were less than 0.05µm apart even small values of chemical shrinkage from the curing process were likely to cause matrix failure between the two fibres, thus providing a site for fibre–matrix debonding to initiate. This study has observed that when fibres are this close and share an interface, the debonding mechanism will favour one fibre over another and continue separating that fibre from the matrix. The debonded region in Fig. 5[b] is similar to what would have developed with further loading at Fig. 5[a].

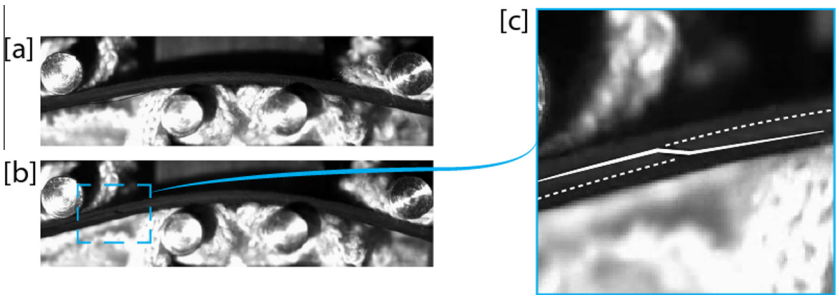

Fig. 3. Still images taken from high speed camera: [a] is the last frame recorded prior to intralaminar failure, while [b] shows the next frame taken just 0.4ms seconds later, where catastrophic failure is observed, shown close-up in [c].

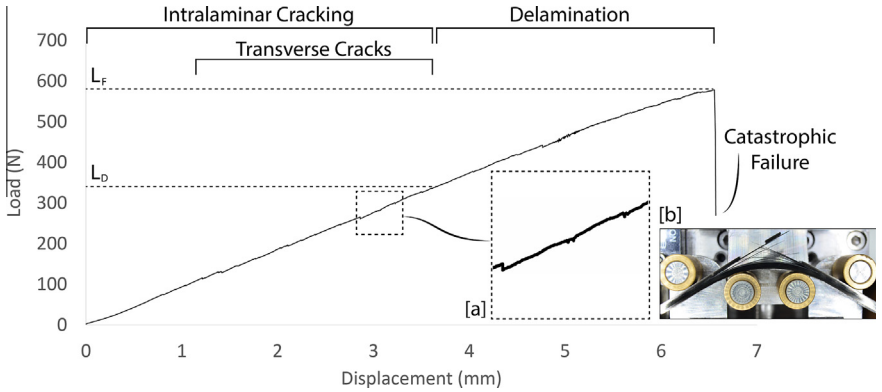

Fig. 4. Typical load/displacement curve for bending of a $[90_4/0_7/90_4]$ laminates. Delamination initiates at L_D, and catastrophic failure occurs at L_F.

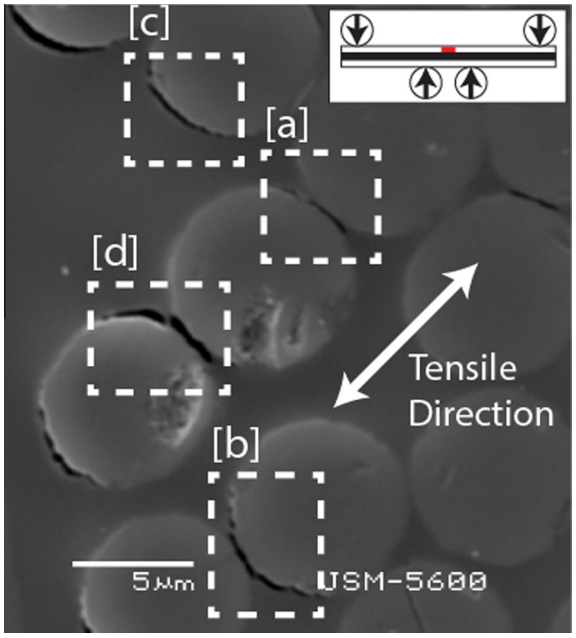

Fig. 5. Debonding locations between fibres at shared fibre/matrix interfaces displaying different debonding mechanisms in a 90° ply.

The debond initiated at a shared interface between two adjacent fibres, favouring the fibre on the right, and continued to debond around the interface of this fibre. From observation of debonds in this study, it was noted that adjacent fibres typically did not develop independent debonds initiating at the same shared interface.

The debond in region Fig. 5[c] is not located at the closest point between two fibres, but located adjacent to a matrix rich region. Failure here is, thus, solely governed by high traction between the fibre and matrix as a result of being aligned with the tensile loading direction. The region highlighted in Fig. 5[d] is a combination of the type of debonds seen at Fig. 5[a] and [c], with two separate debonds forming diametrically opposite, one adjacent to a fibre and the other adjacent to a matrix rich region. As shown, the upper debond is separated by a very fine fibule of matrix of approximately 0.1 μm thickness. As shown later (in Section 3.2.2), these individual debonds eventually coalesce with increasing load.

The behaviour described above was also observed in previous work by other authors. For example, it was found that the interface between the fibre and matrix was the most likely location for failure initiation due to its relative weakness [19]. Smith and Boniface [20] noted that surface defects from laminate manufacturing often encourage the initiation of debonding close to the defect. It has been shown in previous work that residual thermal stresses from the manufacture of the laminate would encourage failure at a region of the fibre–matrix interface facing a large localised concentration of resin due to the local tensile radial stress [21,22]. Along with the tensile loading direction, this also explains the failure shown in Fig. 5[c], which is facing a large resin rich pocket. Martyniuk et al. [7] used X-ray microtomography to show that debonds start at the free surface of the fibre, before extending down along the fibre, through the thickness of the laminate with increased applied loading. Hence, the surface SEM analysis performed here is deemed to be a good measure of failure initiation.

3.2.2. Micro-crack growth

Once sufficient fibre–matrix debonding has taken place, intralaminar failure continues in the form of micro-crack growth. This is the result of debonds growing and coalescing with debonds from other fibres through matrix cracking as shown in Figs. 6–8. In Fig. 6[a] the meandering transverse crack grows from the fibre–matrix interface of one fibre to the next at the closest point between the fibres. The preferred route seen in Fig. 6[a] is not entirely at the fibre–matrix interface, but the gaps between the interfaces are bridged by matrix cracking, indicating that the matrix is the next weakest medium for crack propagation. The two regions marked in Fig. 6[b] show matrix cracks which have continued to grow beyond the fibre–matrix interface into small resin rich pockets. In these particular cases, with increasing load

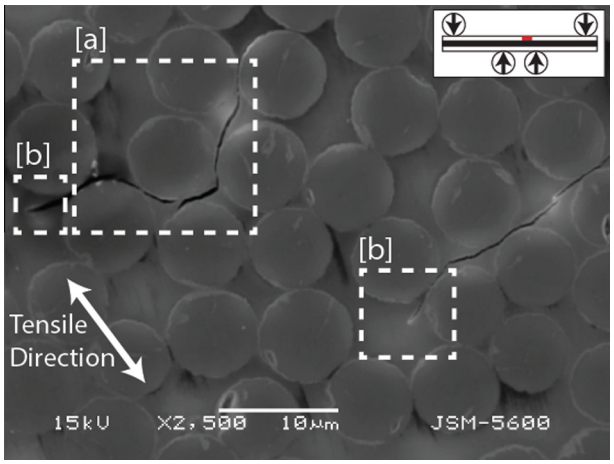

Fig. 6. Cracking at fibre/matrix interfaces connected by matrix cracks, and crack tip growth into resin rich pockets.

the crack tip was seen to propagate through the resin rich pocket to the next nearest favourably debonded fibre–matrix interface.

The regions seen in Fig. 7[a] show similar matrix cracks through resin rich pockets, with abrupt changes in matrix crack path direction due to the crack choosing the most favourable debonded fibre–matrix interfaces. Fig. 7[b] shows the characteristic glow due to specimen charging that occurred at newly exposed portions of the matrix when the crack opened up [17], which was in fact beneficial as it helped identify the location of the crack tip.

In Fig. 8[a], localised regions of significant transverse matrix cracking are seen. In this particular image, the separate micro-cracks have not yet coalesced. Due to the bending load, the left side of the micro-structure is under greater tensile loading than the right, causing transverse cracking to progress from the left to the right. In Fig. 8[b] a number of fibres were observed to have debonded on both their upper and lower surfaces forming small micro-cracks.

3.2.3. Transverse crack arrest

With sufficient loading these aforementioned micro-cracks in the $[90/0]_s$ layup coalesce and form a complete transverse crack, as shown in Fig. 9, and also found in [23]. This transverse crack grows relatively slowly through the 90° plies until it reaches the next alternately orientated ply, in this case the 0° ply block. In general, a completed transverse crack will follow a reasonably straight path from the outer surface of the 90° ply block to the 0° ply block, as seen in Fig. 9. Upon reaching these opposing 0° plies the crack tip will sometimes immediately initiate a local delamination [19]. In other cases, such as that seen in Fig. 9, further loading is required to initiate local delamination at the transverse crack tip.

It was observed in our previous research that once the number of transverse cracks had reached saturation, which varied depending on the 90° ply block thickness, the next damage mechanism to initiate was delamination from the transverse crack tips. It was also noted that not all transverse cracks initiated micro-delamination and instead contributed no further to damage progression.

3.2.4. Delamination

Delamination between the 0° and 90° plies initiates at the point where the 90° transverse crack reaches the 0° plies. With sufficiently low displacement rate of the loading crosshead (33 μm/min) delamination did not initiate immediately. From Fig. 10, it can be seen that delamination at the ply boundary initiates similarly to transverse cracks. Initially, the fibres and matrix debond, generally at the fibre–matrix interface at the closest point to the 0° plies. As loading continues, this debond becomes a void of significant scale, as shown in Fig. 10[a]. The crack tip at Fig. 10[b] is from another similarly debonded fibre, but where the shape has changed from an initially parabolic shaped void (as in Fig. 10[a]) to a more traditional singular crack tip shape. This crack tip is growing through the matrix to meet the debond at Fig. 10[a]. The region marked at Fig. 10[c] shows the next stage, when adjacent crack tips from debonds coalesce at the ply boundary. This "micro-delamination" process continues along the span length of the specimen, parallel to the 0° plies, with the crack tip growing to reach additional debonds as loading is increased. It was also observed in this example that the delamination cracks did not run along the fibre–matrix interface of the 0° plies, but remained as a matrix crack at the earlier and slower stages of delamination. As bending loading increased, the rate of delamination accelerated prior to catastrophic failure, and the delamination rapidly spread further across the span length at the 90°/0° ply boundary.

The progression of delamination from a transverse crack is shown in Fig. 11[a]. The primary delamination in this example is seen in Fig. 11[b]. A typical secondary delamination initiated in the opposite direction, as shown in Fig. 11[c], but the length of secondary delamination was found to be significantly less than

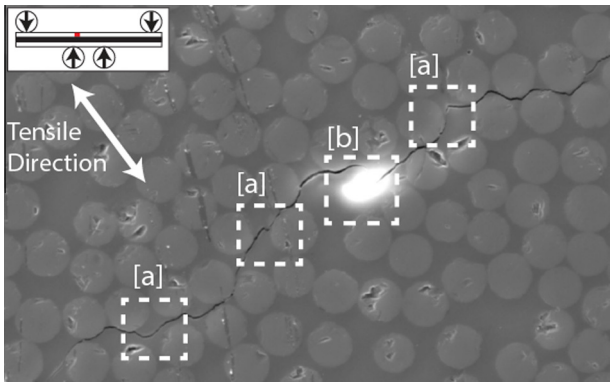

Fig. 7. Matrix cracking and abrupt deflections to fibre/matrix interfaces.

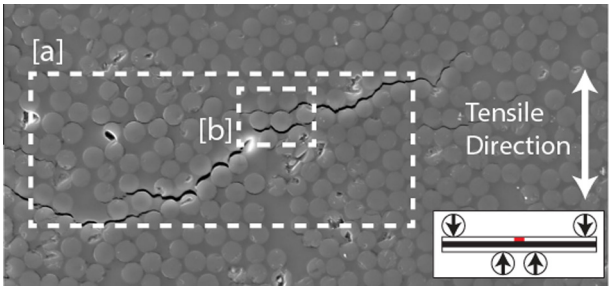

Fig. 8. Intralaminar transverse cracking dominated by fibre/matrix interface failure.

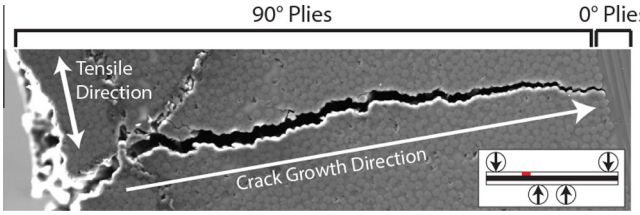

Fig. 9. A completed transverse crack following a relatively straight path through 90° plies. Note that delamination has not initiated immediately and requires further loading.

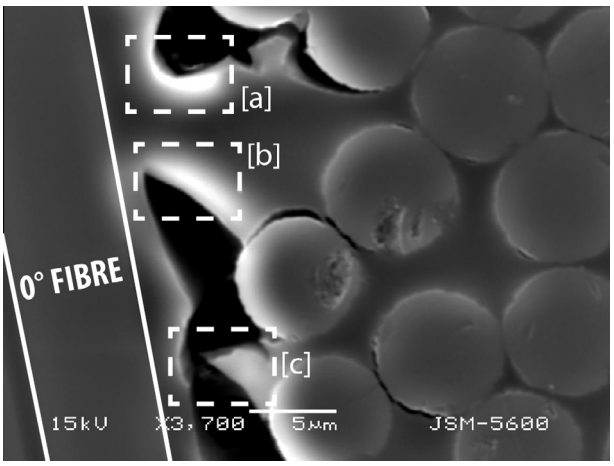

Fig. 10. Micrograph of delamination initiation at the 0°/90° ply boundary.

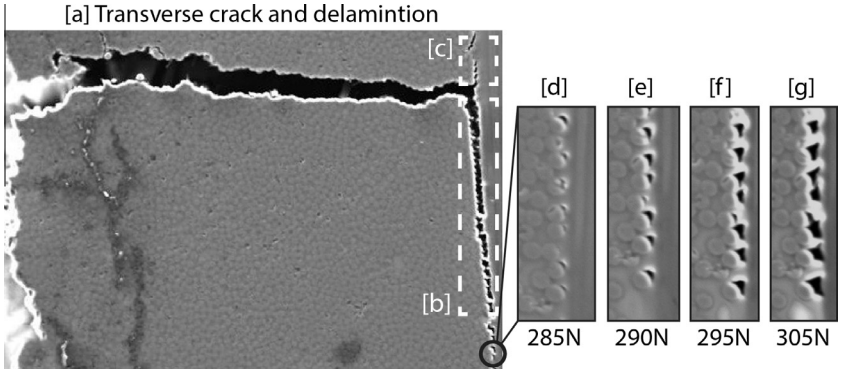

Fig. 11. Micrographs of primary and secondary delamination growth from a transverse crack. Damage progression at the delamination crack tip is shown at higher magnification.

the dominant primary delamination. Many transverse cracks develop delaminations in either direction along the 0° ply boundary. However, generally the primary delaminations were observed to grow away from the centre of the span length towards the support pins. Only for transverse cracks at, or very near, the centre of the span length were there significant delaminations either side of the transverse cracks due to the similar stress states either side of the transverse crack.

Figs. 11[d–g] show higher magnification images of the damage seen at the crack tip at the 90°/0° boundary delamination. The progression of this damage is seen at various load levels from the initiation of fibre–matrix decohesion at 285 N to major void development at 305 N, prior to void coalescence. At 305 N, the voids are separated by matrix fibules at the 90°/0° ply boundary, and with further loading these fibules break and the delamination progresses further. In all our experiments, this characteristic 'tearing' occurred at the crack tips for steady growth 90°/0° boundary delaminations in bending of $[90/0]_s$ laminates, prior to rapid delamination at catastrophic failure.

3.2.5. 0° Fibre breakage

Prior to transverse cracking and delamination, small scale damage was observed in the 0° ply block in the form of fibre breakage, such as those shown in Fig. 12. Observations of fibre failure on the laminate surface should be addressed carefully, bearing in mind the reduction in cross sectional area of the fibres at the surface during specimen preparation. Fig. 13 shows similar fibre breakage

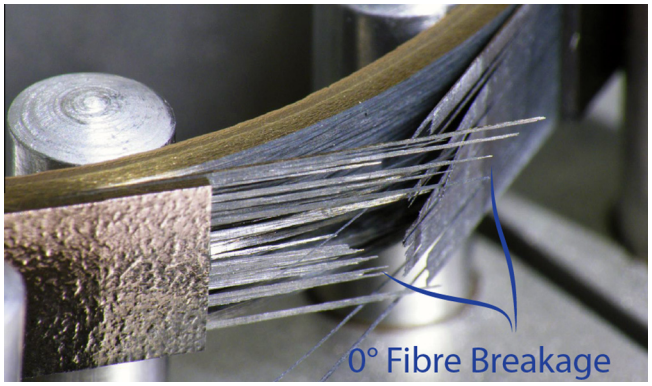

Fig. 13. Macro photography showing many clusters of broken fibres seen through the bulk of the laminate under four-point bending.

though the thickness of the laminate for a specimen under a bending load. This indicates that fibre breakage observed at the surface of the laminate is representative of the bulk behaviour of the laminate and is not purely the result of damaging fibres at the surface during the polishing process.

The normal tensile stress in the 0° plies furthest from the loading pin was significant enough to cause fibre breakage. It was observed in Fig. 12[a] that the concentration of fibre breakage increased from right to left across the 0° ply block due to the linear

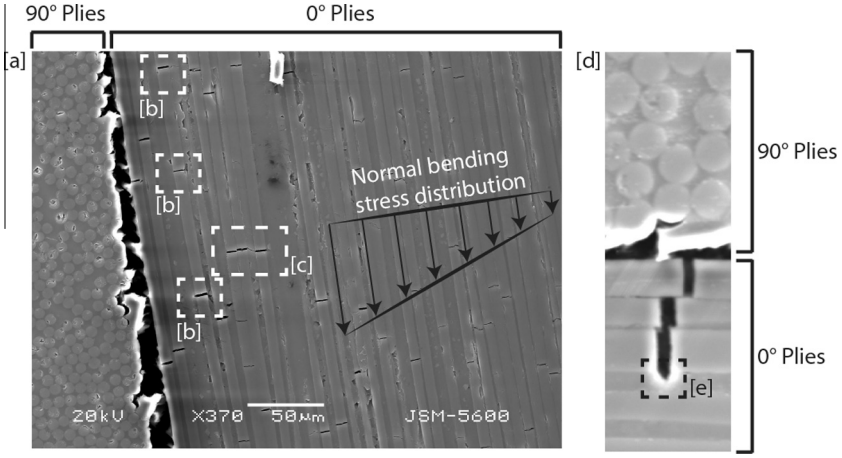

Fig. 12. Significant fibre breakage in 0° plies seen in two samples. Both illustrate regions where cracks in 0° fibres initiate further cracking in adjacent fibres and through the matrix.

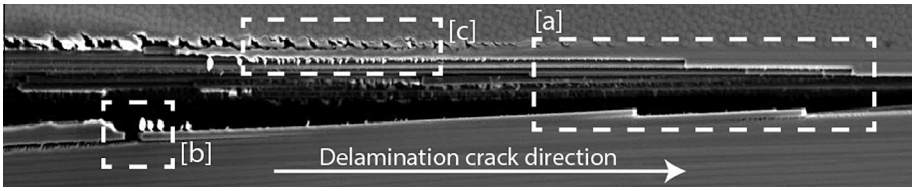

Fig. 14. Intra-ply delamination in the 0° ply block, following a step-like path through existing fibre breakages.

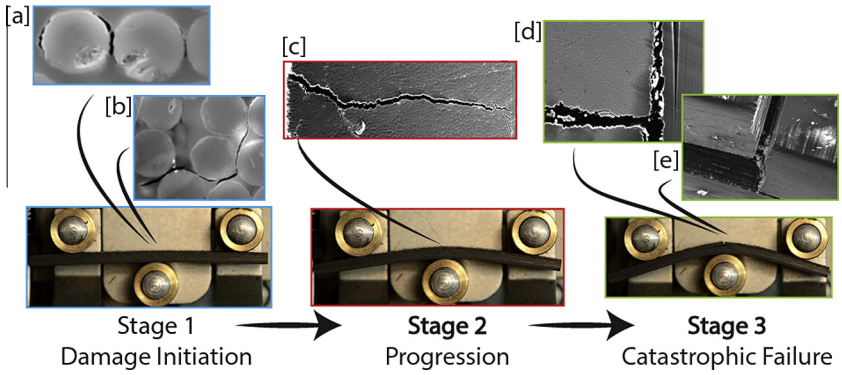

Fig. 15. Stages of damage in bending, from damage initiation to catastrophic failure.

increase in normal bending stress, as the distance away from the neutral bending axis (i.e. the centre of the laminate) increased, as expected. In Fig. 12[b], it can be seen that an individual fibre breaks in a number of locations, less than 100 μm apart. This is characteristic of many of the fibres seen in the high tensile stress region, indicating that the tension remained high along the length of the fibres even after they broke, which is caused by stress transfer into the surrounding matrix and back into the fibre. The load–displacement data gathered from the micro-tester did not show any significant or observable indications of damage at these fibre failure events. In Fig. 12[c], three fibres break in the same region, indicating an interaction of the stress fields at this fibre breakage region. The fibre on the left of Fig. 12[c] most likely broke first due to the greater tensile stress, and the localised stress concentration which developed from this initiated the breakage of the next fibre to the right. A thin matrix crack is then seen to connect the break from the second fibre to the third, which also broke. Similar to Fig. 12[c], Fig. 12[d] from another specimen, shows slightly staggered 0° fibre breakage, which are all joined together through cracks in the matrix. The crack tip is also clearly visible, growing through the matrix and into the next fibre (Fig. 12[e]) in a progressive manner. The difference seen in Fig. 12[e] when compared with Fig. 12[c] is that the fibre break has occurred at the ply boundary between the 0° and 90° plies, which meant that a delamination crack at this boundary had the potential to deflect perpendicularly to the loading direction and through the 0° ply block.

The joining of a delamination crack at a 90°/0° boundary to a fibre crack in the 0° ply block could also cause the delamination to continue along the fibre–matrix interface of the 0° fibres, similar to the behaviour shown in Fig. 14. In this image, a 90°/0° boundary delamination has joined with the fibre breaks in the 0° plies, and continued the delamination in the 0° ply block. In Fig. 14[a], the step-like path of this delamination is evident. Each time the delamination crack reaches the next 0° fibre breakage, the delamination steps down through the thickness of the 0° ply block. Fig. 14[a] shows two steps in the delamination crack path and the upper and lower edges after separation. At this stage in the laminate failure sequence, the structure has lost most of its load bearing capacity as the material simply peels apart with further loading. The damage at Fig. 14[b] shows a 0° fibre breakage and debonding crack growth along the length of the fibre left and right of the fibre breakage. The area in Fig. 14[b] was the original location of the change from 90°/0° boundary delamination, to cracking in the 0° ply block. The area in Fig. 14[c] shows the characteristic 'tearing' at the 90°/0° boundary at the crack tip of the boundary delamination, similar to the damage shown previously in Fig. 11[d–g]. This damage occurred prior to the development of the step-like crack path in the 0° ply block (shown in Fig. 14[a]).

4. Conclusions

The entire failure sequence for $[0_4/90_7/0_4]$ and $[90_4/0_7/90_4]$ laminates was observed using in-situ SEM micro-mechanical testing. In testing of $[0_4/90_7/0_4]$ laminates, there were no significant signs of damage prior to catastrophic shear stress dominated failure which completed in under 0.4 ms. This constrained cracking mechanism, where micro-damage was suppressed prior to total structural failure, should be considered at the design stage by choosing a suitable constraining ply layup configuration to prevent early development of micro-cracks and associated leakage.

In this study it was found that the first stage of damage in the intra-ply region of a $[90_4/0_7/90_4]$ laminate in bending was fibre–matrix interfacial debonding (Fig. 15[a]). This was observed to be influenced by the proximity of fibres and the loading direction. Debonds coalesce by cracking through the matrix to form micro-cracks (Fig. 15[b]). Further progression of the crack follows the path of least resistance either at the fibre–matrix interface or through the matrix. With sufficient loading, micro-cracks coalesce and form complete transverse cracks which grow to meet the boundary of the next alternately orientated ply (Fig. 15[c]). Eventually, this leads to the onset of delamination (Fig. 15[d]) and subsequent catastrophic laminate failure (Fig. 15[e]). Much effort is urgently required to integrate intralaminar damage with interlaminar damage, as to date they are mostly treated incorrectly as independent damage mechanisms, and this paper may be useful to provide fundamental insight into the physics of interaction of these damage mechanisms.

Acknowledgements

This publication has emanated from research conducted with the financial support of Science Foundation Ireland under Grant Number SFI 13/IA/1833.

References

[1] Crossman F, Wang A. The dependence of transverse cracking and delamination on ply thickness in graphite/epoxy laminates. Damage Compos Mater 1982:118–39.
[2] Nairn JA. Material performance. Micromechanical modeling of composite fracture. In: Wang SS, Fitting DW, editors. Compos. Mater. Offshore Oper. Proc. First Int. Work. Houston: U.S. Department of Commerce, Technology Administration, National Institute of Standards and Technology; 1993. p. 175–6.
[3] Kevin R, Joseph S, Sankara S. Detection of micro-leaks through complex geometries under mechanical load and at cryogenic temperature. In: 19th AIAA Appl. Aerodyn. Conf.. Anaheim: American Institute of Aeronautics and Astronautics; 2001.
[4] Nairn JA, Hu S. The initiation and growth of delaminations induced by matrix microcracks in laminated composites. Int J Fract 1992;57:1–24.
[5] Tong J, Guild FJ, Ogin SL, Smith PA. On matrix crack growth in quasi-isotropic laminates—I. Experimental investigation. Compos Sci Technol 1997;57:1527–35.
[6] Sebaey TA, Costa J, Maimí P, Batista Y, Blanco N, Mayugo JA. Measurement of the in situ transverse tensile strength of composite plies by means of the real time monitoring of microcracking. Compos Part B Eng 2014;65:40–6.
[7] Martyniuk K, Sørensen BF, Modregger P, Lauridsen EM. 3D in situ observations of glass fibre/matrix interfacial debonding. Compos Part A Appl Sci Manuf 2013;55:63–73.
[8] Mortell DJ, Tanner DA, McCarthy CT. In-situ SEM study of transverse cracking and delamination in laminated composite materials. Compos Sci Technol 2014;105:118–26.
[9] Hobbiebrunken T, Hojo M, Adachi T, De Jong C, Fiedler B. Evaluation of interfacial strength in CF/epoxies using FEM and in-situ experiments. Compos Part A Appl Sci Manuf 2006;37:2248–56.
[10] Naseem K, Yang Y, Luo X, Huang B, Feng G. SEM in situ study on the mechanical behaviour of SiCf/Ti composite subjected to axial tensile load. Mater Sci Eng, A 2011;528:4507–15.
[11] Gutkin R, Pinho ST, Robinson P, Curtis PT. On the transition from shear-driven fibre compressive failure to fibre kinking in notched CFRP laminates under longitudinal compression. Compos Sci Technol 2010;70:1223–31.
[12] Parvizi A, Garrett KW, Bailey JE. Constrained cracking in glass fibre-reinforced epoxy cross-ply laminates. J Mater Sci 1978;13:195–201.
[13] Bader MG, Boniface L. The assessment of fatigue damage in CFRP laminates. In: Feest T, editor. Proc. Int. Conf. Testing, Eval. Qual. Control Compos. Guildford: Butterworths; 1983. p. 66–75.
[14] Liu S. Delamination and matrix cracking of cross-ply laminates due to a spherical indenter. Compos Struct 1993;25:257–65.
[15] Shyr T-W, Pan Y-H. Impact resistance and damage characteristics of composite laminates. Compos Struct 2003;62:193–203.
[16] Parvizi A, Bailey JE. On multiple transverse cracking in glass fibre epoxy cross-ply laminates. J Mater Sci 1978;13:2131–6.
[17] Hinz S, Omoori T, Hojo M, Schulte K. Damage characterisation of fibre metal laminates under interlaminar shear load. Compos Part A Appl Sci Manuf 2009;40:925–31.
[18] Maligno AR, Warrior NA, Long AC. Effects of inter-fibre spacing on damage evolution in unidirectional (UD) fibre-reinforced composites. Eur J Mech A/Solids 2009;28:768–76.
[19] Greenhalgh E, Hiley M, Meeks C. Failure analysis and fractography of polymer composites. 1st ed. Cambridge: Woodhead Publishing Limited; 2010.
[20] Smith PA, Boniface L, Glass NFC. A comparison of transverse cracking phenomena in (0/90)s and (90/0)s CFRP laminates. Appl Compos Mater 1998;5:11–23.
[21] Gentz M, Armentrout D, Rupnowski P, Kumosa L, Shin E, Sutter JK, et al. In-plane shear testing of medium and high modulus woven graphite fiber reinforced/polyimide composites. Compos Sci Technol 2004;64:203–20.
[22] Sjogren A. Matrix and interface effects on micro-cracking in polymer composites, 1997.
[23] Berthlot JM. Composite materials: mechanical behavior and structural analysis. 1st ed. New York: Springer; 1999.